IEEE Access
Multidisciplinary | Rapid Review | Open Access Journal

Received 1 May 2023, accepted 19 May 2023, date of publication 29 May 2023, date of current version 9 June 2023.

Digital Object Identifier 10.1109/ACCESS.2023.3281197

RESEARCH ARTICLE

Adaptive Rate Polar Code for DCT-Based Digital Image Transmission

MAI ADEL[1], SALWA H. EL-RAMLY[2], (Life Senior Member, IEEE), AND BASSANT ABDELHAMID[2], (Senior Member, IEEE)

[1]Department of Mathematics, German University in Cairo, Cairo 12613, Egypt
[2]Electronics and Communications Department, Faculty of Engineering, Ain Shams University, Cairo 11517, Egypt

Corresponding author: Mai Adel (mai.ebrahim@guc.edu.eg)

ABSTRACT Polar code is a recent forward error correction technique that is characterized by its low encoding/decoding complexity and good error performance. In this paper, a complete image transmission system (transmitter and receiver) is proposed to improve the image quality over different types of channels such as Gaussian, Rayleigh and Rician channels. The proposed system is based on encoding the most significant quantized Discrete Cosine Transform (DCT) coefficients of the digital image using adaptive rate polar coding, by changing the number of frozen bits depending on the number of significant DCT coefficients that depend on the channel quality. Simulation results reveal that the proposed system achieves better performance compared to the coded digital transmission schemes in terms of the Structural SIMilarity (SSIM) index and the Peak Signal to Noise Ratio (PSNR) for different sizes of images. Moreover, it is not subject to ''cliff effect'' and exhibits improvement in image quality according to the channel quality.

INDEX TERMS Adaptive rate, cliff effect, DCT, frozen bits, image transmission, polar code.

I. INTRODUCTION

In the current era, ubiquitous systems, including social media, healthcare applications, cloud-based data storage systems, and the Internet of Things (IoT), are widely employed where digital images are the most popular transmitted data in such systems [1]. Many interesting applications are incorporating digital images such as the crop disease prediction [2], biometric authentication [3], content-based image retrieval [4]. To establish a reliable digital image transmission, traditional communication systems first employ image compression with a source coding algorithm [5]. Since the frequency domain is more stable and impervious to manipulation than spatial domain [6], [7], Discrete Cosine Transform (DCT) can be utilized to convert images from spatial to frequency domain. JPEG [8] is the most common standard that applies DCT followed by quantization and entropy encoding to encode the images [9]. Then, the bit stream is encoded by near-optimal channel codes (e.g., Low-Density Parity Check (LDPC), Turbo codes) to approach the theoretical optimality [10]. However, traditional digital-based transmission scheme performance severely degrades with the channel variations [11]. When the channel Signal-to-Noise Ratio (SNR) deteriorates below a certain threshold, the channel noise and impairments might result disastrous errors for entropy decoding leading to a considerable degeneracy of the received image fidelity, this is known as the ''cliff effect'' [11]. Beyond this threshold, the performance reaches its bottleneck, and the received image quality remains constant [12], unless an adaptive rate control of source and channel coding is executed according to the channel variations [13]. To resolve this problem, Joint Source Channel Coding (JSCC) and adaptive rate channel coding are introduced.

JSCC schemes based on Double Protograph LDPC (DP-LDPC) for DCT-based image transmission are proposed [14], [15], and [16], where P-LDPC code is utilized for source and channel coding. However, DP-LDPC system is sensitive to the source entropy, it suffers from high error floor while transmitting source sequence with high entropy. In [14], the image pre-processing is adopted before JSCC to improve the error performance of DP-LDPC codes.

The associate editor coordinating the review of this manuscript and approving it for publication was Jeon Gwanggil.

This pre-processing technique adds more processing time to the system. On the other hand, in [15], joint optimization method and fuzzy logic control rate allocation of DP-LDPC codes for IoT scenarios are utilized. However, the authors claimed that the optimization method needs improvement and more practical channels must be considered. In recent study [16], authors proposed stopping criterion to reduce the decoding complexity of DP-LDPC JSCC system in image transmission. However, the authors utilized two transmission schemes for the source sequences that increase the system complexity. Alternative strategy considers Unequal Error Protection (UEP) based on different priorities of the transmitted data, UEP systems have been designed using turbo codes [17] and P-LDPC code [18]. However, turbo and LDPC decoding are highly computationally intensive tasks which make the previously proposed systems not suitable for some 5G applications.

On the other hand, the concept of adaptive rate coder is an efficient solution to achieve the best performance of data communication under varying the channel conditions [19]. A variety of adaptive forward error correction techniques for image transmission have been proposed [20], [21]. In [20], the authors proposed adaptive Reed-Solomon (RS) codes for image transmission in wireless sensor networks, however the image in the spatial domain was processed. The authors in [21] utilized adaptive convolution coding and cooperative relayed for image transmission. However, high power consumption of convolution decoders makes it unsuitable for IoT devices [22].

Polar codes were introduced in 2009 by Arikan [23], these codes are characterized by their low encoding and decoding complexity, their competitive reliability and having very low latency. This fosters their employment for low powered devices such as IoT applications and Ultra-Reliable and Low-Latency Communication (URLLC) systems [24]. Polar codes are considered the first Shannon channel capacity-achieving codes [23]. Recently, they are adopted for control channels in the 5G enhanced Mobile Broad Band (eMBB) scenario as stated by 3rd Generation Partnership Project (3GPP) [25]. In addition, studies in [26] and [27] have shown that in the context of 5G test scenarios, polar codes perform better than LDPC and turbo codes. Recently, authors in [28] showed that polar codes have outstanding results in terms of decoding latency compared to LDPC codes. In addition, they demonstrated that the computational complexity of coding and decoding of polar code is less than the complexity of LDPC with BCH codes. Moreover, the adaptability rate of polar codes allows them to be widely used for ongoing 5G applications [29].

Polar codes for image transmission have gained prominence through many studies [30], [31], [32], [33], [34], [35], [36], [37]. The performance of polar coded image transmission over Rayleigh channel was discussed in [30]. The results prove that it has better performance than LDPC in terms of Peak Signal to Noise Ratio (PSNR). Authors in [31] studied the transmission of JPEG2000 images over Additive White Gaussian Noise (AWGN) channel. Results showed that polar codes have better performance than LDPC codes. In [32], polar codes performance was investigated for image transmission system over AWGN channel using OFDM modulation and compared with BCH coding. The results showed that the received polar-coded image has better quality than BCH-coded one. Authors in [33] utilized the channel polarization property of polar codes to achieve UEP of JPEG2000 stream over AWGN channel. Moreover, UEP using polar codes for original image was exploited in [34] and [35]. The quality of polar-coded images in the spatial domain transmitted over AWGN channel was investigated in [36], authors showed the robustness of polar codes at low SNR. Recently, authors in [37] modeled a 3D and 2D polar-coded image transmission system over Rician channel only for certain values of Rician factor. Results indicate that polar-coded system achieves better image quality than RS-coded system.

As far as authors know, the application of polar codes to DCT-based image coder is not tackled yet in literature. Therefore, we propose in this paper DCT-based image transmission by adaptive rate polar code based on the channel quality. Unlike previous works [15], [17], [18], in this paper, all transmitted DCT coefficients are equally protected. Moreover, non-significant DCT coefficients are disregarded and adaptively determined in the transmitter according to predesigned lookup table based on the channel quality. The aim is to achieve a graceful reception of the transmitted image and avoid ''cliff effect''. Table 1 summarizes the aforementioned works for digital image transmission and the proposed system.

The main contributions of this paper are summed up as follow:

i) Propose a general DCT-coded image transmission system using an adaptive rate polar code for any image size to avoid ''cliff effect'' phenomena. Moreover, the proposed polar code construction is based on 5G reliability sequence.
ii) Design a look-up table that stores the best number of transmitted DCT coefficients for different channel qualities. Offline designed look-up table avoids delay associated with real time optimization techniques which makes the system suitable for real time applications. This, in turn, increases the battery lifetime of portable devices.
iii) Propose the utilization of frozen bits in the image transmission, to replace the non-transmitted DCT coefficients. This reflects on the receiver side by avoiding zero padding for the decoded frozen bits.
iv) Find a model for the relationship between channel quality and Rician fading factor to easily construct a look-up table for different fading factor values.

The rest of the paper is organized as follows: Section II presents the system model, and the detailed description of the proposed transmitter and receiver are presented in

TABLE 1. Comparison of previous work with the proposed system.

Ref.	Image processing domain	Source encoder	Channel encoder	Channel model	Source/channel rate adaption Criteria	Test image size
[20]	Spatial	No	Reed- Solomon (RS)	Log-normal shadowing model	Distance between nodes in smart grid	Not mentioned
[21]	Wavelet transform	Embedded Zero-tree Wavelet	Convolution codes	AWGN Rayleigh	Channel quality	256×256
[30]	Spatial	No	Polar /LDPC	Rayleigh	No	256×256
[31]	Spatial	JPEG2000	Polar/LDPC	AWGN	No	Not mentioned
[32]	Spatial	No	Polar/BCH	AWGN	No	512×512
[33]	Spatial	JPEG2000	Polar UEP	AWGN	No	512×512
[34]	Spatial	No	Polar UEP	AWGN	No	512×512
[35]	Spatial	No	Polar UEP	AWGN	No	512×512
[36]	Spatial	No	Polar	AWGN	No	256×256
[37]	Spatial 3D point cloud	No	Polar	Rician (k =4) Rician (k =2)	No	Not mentioned
[14]	DCT	P-LDPC	P-LDPC	AWGN	No	512×512
[15]	DCT	P-LDPC	P-LDPC	Time invariant and time-varying AWGN	Importance of each frame and real time channel condition	256×256
[16]	DCT	P-LDPC for some frames	P-LDPC	AWGN	No	512×512
[17]	DCT	No	Turbo UEP	AWGN	No	Not mentioned
[18]	DCT	P-LDPC	P-LDPC	AWGN	No	800×800
Proposed	DCT	No	Polar using 5G reliability sequence	AWGN Rician (k=1:10) Rayleigh	Channel quality	256×256 480×480 512x512

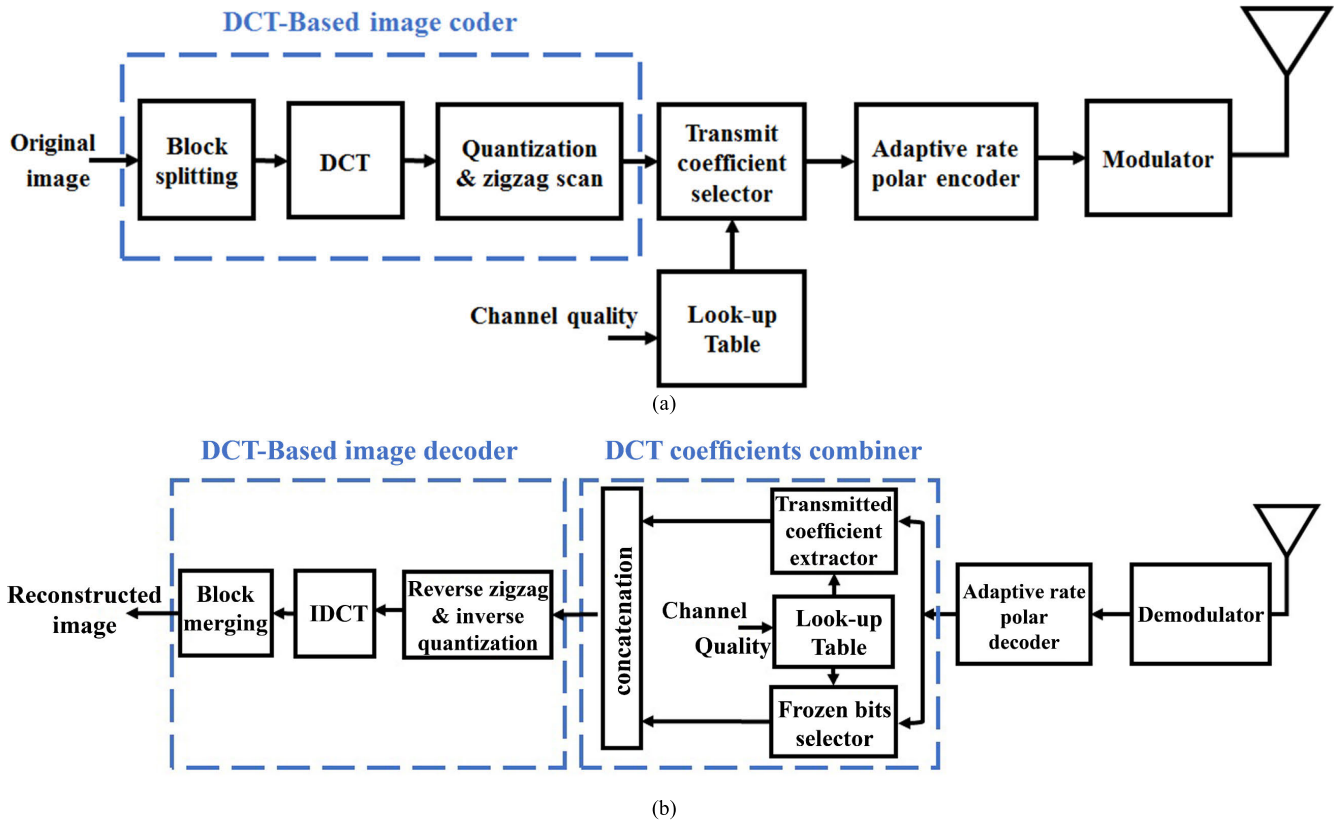

FIGURE 1. Proposed DCT-based image communication system: (a) proposed transmitter; (b) proposed receiver.

this section. Simulation results and comparative analysis are provided in Section III. Finally, the paper is concluded in Section IV.

II. SYSTEM MODEL

In this section, a new digital image transmission system is proposed. The proposed system model is demonstrated in Fig. 1. The following subsections illustrate the proposed transmitter and receiver in detail. In the proposed system, the channel quality is assumed to be known at both the transmitter and the receiver.

A. PROPOSED TRANSMITTER

The original image is fed to the transmitter shown in Fig.1a to be transmitted over the communication channel. Initially, the image in the spatial domain is transformed to the frequency domain through DCT-based image coder. The detailed functionality of each block is described in the following subsections.

1) DCT-BASED IMAGE CODER

The DCT-based image coder block diagram is shown in Fig.1a, which has the original image as an input, and outputs a vector of DCT coefficients. This coder is composed of the same blocks as standard JPEG without entropy encoding. The functionality of each block is described as follows:

Block splitting: The original A×A image is divided into non-overlapping blocks of size 8 × 8 pixels. Hence, the total number of blocks ($B = A^2/64$), where A (pixels) is the length and width of the image.

DCT: The DCT in [38] is individually employed for each block. The key characteristic of the DCT transform is the focus of the signal energy into a small portion of the coefficients at the top left part of the block (low frequency components), and it has a quick decline of the amplitude of the DCT coefficients from the low frequency to the high frequency regions (bottom right).

Among all the 64 coefficients per block, the average intensity of the block is represented by the first coefficient, which has the largest magnitude and is called the DC coefficient. On the other hand, the first 21 coefficients including the DC coefficient; are named Low Frequency (LF) coefficients and represent the basic information of the image, while the remaining 43 coefficients are named High Frequency (HF) coefficients and represent the image details [15]. To intuitively realize the significance of the LF coefficients, consider *Lena*'s image as an example. Fig.2 illustrates the visual result when the *Lena* image is rebuilt for different number of coefficients using DCT-based image coder and decoder.

Clearly, keeping only the DC coefficient from each block mirrors the basic element of the image (Fig.2b). Besides, image reconstruction using only LF coefficients leads to

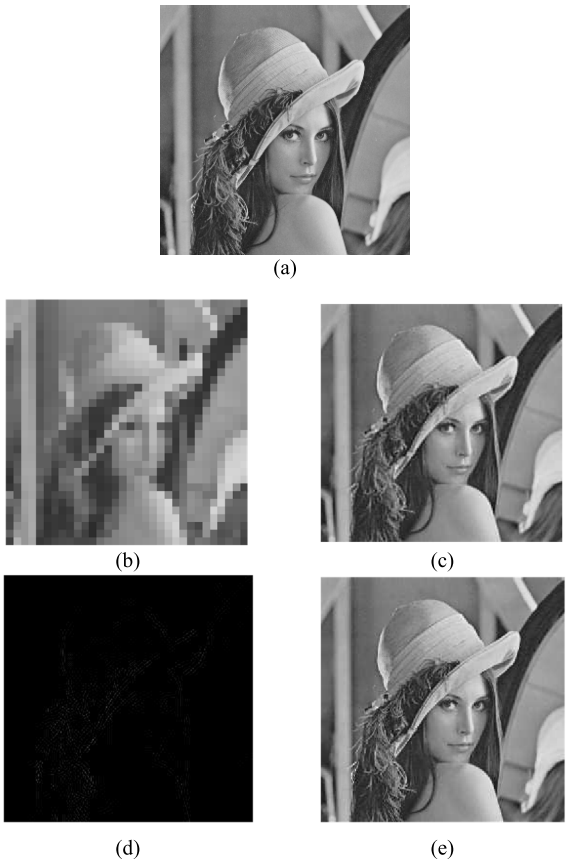

FIGURE 2. Image reconstruction using different number of DCT coefficients: (a) Original Image; (b) Using only DC coefficient; (c) Using 21 LF coefficients; (d) Using 43 HF coefficients; (e) Using all 64 coefficients.

unnoticeable information loss (Fig.2c). On the contrary, the reconstructed image using only HF coefficients in Fig.2d is severely damaged. Surely, utilizing both HF and LF coefficients without errors in the reconstruction process leads to no information loss. As a result, LF coefficients are very vital for the reconstruction process. On the other hand, HF coefficients can be considered as supplementary information to enhance the quality of image and to show the edges inside the image.

Quantization and zigzag scan: Quantization is employed to compress the information in the frequency domain. The default luminance quantization table in [8] is utilized such that the HF coefficients are more heavily compressed than the LF coefficients; hence, more zeros exist in the high frequency area with minimal effect on the image quality.

Lastly, the quantized coefficients are ordered according to the zigzag pattern in [8]. Thus, the coefficients are sequenced in descending order according to their importance (LF coefficients followed by HF coefficients).

2) TRANSMIT COEFFICIENT SELECTOR

The ordered DCT coefficients vector for each block and a look-up table value are fed to the transmit coefficient selector as depicted in Fig.1a. This selector aims to only select the pre-defined number of DCT coefficients per block that are transmitted according to the look-up table. The proposed system transmits LF under all channel quality, and adaptively considers some HF coefficients according to the channel quality to improve the quality of the received images under all channel conditions. The pre-designed look-up table that contains the best number of coefficients for a set of possible channel quality is utilized as will be illustrated in subsection C. The selected coefficients are then represented by 8-bits and considered as source sequence of length M for the channel encoder, where M is variable according to the number of selected coefficients.

3) ADAPTIVE RATE POLAR ENCODER

The (N, M) polar encoder is used to transmit the source bits over a communication channel. Its code rate is defined by R which equals M/N, where M is the number of information bits and N is the codeword length and equals 2^n where n is any positive integer. Polar code divides N synthetic channels into M reliable channels and N-M noisy channels. let F be the information set that holds M channel indices. Consequently, the information bits are assigned to the most reliable M channels, while N-M bits are assigned to noisy channels and called frozen bits.

The codeword $\boldsymbol{C}$ of length N is generated as follows [25]:

$$\boldsymbol{C} = \boldsymbol{u}\boldsymbol{G}_N \tag{1}$$

where $\boldsymbol{u} = [u_1, \ldots.., u_N]$ is the input vector generated by sorting the information bits at entries i $\in F$, and setting the frozen bits to zero. $\boldsymbol{G}_N$ is the generator matrix and defined as the n-th kronecker product of Arikan [23] kernel matrix $\boldsymbol{G_2} = \begin{bmatrix} 1 & 0 \\ 1 & 1 \end{bmatrix}$, The generator matrix is mathematically denoted by $\boldsymbol{G}_N = \boldsymbol{G_2}^{\otimes n}$, and is calculated as [25]:

$$\boldsymbol{G}_N = \begin{bmatrix} G_{N/2} & 0 \\ G_{N/2} & G_{N/2} \end{bmatrix} \tag{2}$$

However, code construction methods depend on the channel conditions that increase the coding latency. Recently, the 5G standardization proposed a unique universal channel reliability sequence to be used to extract the individual reliability sequence for each polar code considered in 5G [25]. This sequence consists of 1024-bit channels in an ascending reliability order [39]. It can be utilized to design any 1024 or shorter polar code length. The standard reliability sequence is employed to construct the polar code in our proposed system.

The selected binarized coefficients are considered as the information bits M of the polar encoder, and the code length N is kept fixed. Therefore, according to the selected number of CoeFficients (CFs) from the pre-designed look-up table, M varies adaptively which in turn leads to a variable polar code rate. Finally, the codeword is modulated and transmitted through the communication channel. It is to be noted that the size of the original image has no effect on the information size of the adaptive rate polar encoder since the proposed transmitter is based on image blocks.

B. PROPOSED RECIEVER

On the receiving side, the transmitter operations are inverted and executed in reverse order to reconstruct the image. The proposed receiver block diagram is shown in Fig.1b, and the detailed description is as follows:

1) ADAPTIVE RATE POLAR DECODER

The Successive Cancellation (SC) decoder [23] is proposed since it is favored for its low complexity. The SC decoder tries to estimate the input vector from the received noisy version of the code words $\mathbf{Y}= [y_1, \ldots, y_N]$. Log-Likelihood Ratio (LLR) for u_i is computed as follows:

$$LLR\,(u_i) = ln\frac{P(u_i = 0|\boldsymbol{Y}, u_{i-1})}{P(u_i = 1|\boldsymbol{Y}, u_{i-1})} \tag{3}$$

The information bit is estimated by the decision as:

$$\hat{u}_i = \begin{cases} 0, LLR\,(u_i) \geq 0 \\ 1, LLR\,(u_i) < 0 \end{cases} \tag{4}$$

On the other hand, frozen bits are permanently decoded as zeros.

2) DCT COEFFICIENTS COMBINER

This block has two inputs: the decoded N bits and the look-up table value according to the channel quality. This combiner is composed of a transmitted coefficient extractor, a frozen bit selector, and a concatenator block. Each of these blocks is described as follows:

Transmitted coefficient extractor: To recover the original image, 64 DCT coefficients are required to be decoded from the received data. Since the output of the extractor block depends on the number of significant DCT coefficients, thus the remaining missed coefficients require another processing to be defined, which is done through the frozen bits selector.

Frozen bit selector: When the decoded information bits are less than 512 bits. The decoded frozen bits are utilized to account for the non-transmitted coefficients.

Concatenator: The selected frozen bits are concatenated with the decoded information bits in order to construct a complete image block of 512 bits. Hence, there is no need to pad additional data at the receiver and exploit the decoded frozen bits as zero DCT coefficients.

3) DCT-BASED IMAGE DECODER

The decoded image block bits are converted to decimal values, representing DCT coefficient vectors [17]. To reconstruct the received image, reverse zigzag and inverse quantization are applied to the received DCT coefficients vector [18]. Finally, the inverse DCT in [38] is performed to convert from frequency domain to spatial domain and hence, the digital image is recovered at the terminal end [18].

C. LOOK-UP TABLE DESIGN

As mentioned earlier, the look-up table is utilized in the proposed system to determine the best number of DCT coefficients that are required to be transmitted to maximize the quality of the received image according to the channel quality. Two different image quality metrics are computed to evaluate the received image quality, PSNR and Structural SIMilarity (SSIM). The PSNR, expressed in dB, compares the original image and the reconstructed image according to the pixel intensity, high PSNR denotes that the two images are close. However, PSNR does not perceive the human visual system and is generally defined by Mean Square Error (MSE). PSNR is calculated as [31]:

$$PSNR = 10\log_{10}\left(\frac{255^2}{MSE}\right) \tag{5}$$

where MSE $= \frac{1}{A\times A}\sum_{a=1}^{A}\sum_{b=1}^{A}\|I\,(a,b) - R(a,b)\|^2$, such that $I\ (a,b)$ is the original image of dimension A×A and $R(a,b)$ is the reconstructed image and a, b represent pixel coordinates [35].

On the other hand, SSIM [40] is computed taking the structural information of the image into account, and so the visual quality is considered [32]. The SSIM between the original image I and the reconstructed image R is defined as [40]:

$$SSIM\,(I,R) = \frac{(2\mu_I\mu_R + C_1)(2\sigma_{IR} + C_2)}{(\mu_I^2 + \mu_R^2 + C_1)(\sigma_I^2 + \sigma_R^2 + C_2)} \tag{6}$$

where $\mu_I, \mu_R, \sigma_I, \sigma_R$ and σ_{IR} are the means, standard deviations, and cross covariance of original and reconstructed images, respectively. Constants C_1 and C_2 are included to avoid zero denominators when $\mu_I^2 + \mu_R^2$ or $\sigma_I^2 + \sigma_R^2$ are close to zero. For grey images, the default values of these constants are $C_1 = (0.01 \times 255)^2$ and $C_2 = (0.03 \times 255)^2$ [40]. SSIM values lie in the range (0,1). The closer the SSIM to unity, the higher perceptual similarity between original and reconstructed images.

A detailed study has been performed by varying the number of CFs and E_b/N_o of the channel to determine the best number of CFs. The following subsections demonstrate the construction steps of the look-up table in case of AWGN, Rayleigh, and Rician channels.

1) AWGN LOOK-UP TABLE

Since LF coefficients are transmitted under all channel quality and the maximum number of CFs is 64. Therefore, to construct look-up table, the number of CFs is varied from 21 to 61 coefficients and E_b/N_o is varied from 0 to 3.5 dB.

For each number of CFs and E_b/N_o, the PSNR and SSIM for different grey images are computed. As stated before, the maximum image fidelity is obtained when all coefficients are transmitted, therefore, the max PSNR and max SSIM are computed for each E_b/N_o when the number of CFs = 64 coefficients. For a given E_b/N_o, the difference between PSNR and max PSNR is denoted by Δ PSNR as well as the difference between SSIM and max SSIM is denoted by Δ SSIM are calculated for every number of CFs. The best CFs number is the value at which maximum Δ PSNR and maximum Δ SSIM are obtained. Algorithm 1 summarizes the steps to design look-up table for AWGN channel.

Algorithm 1 Look-up Table Design for AWGN Channel

Inputs: Grey scale image dataset
Outputs: Best number of DCT coefficients (CFs) for each (E_b/N_o), look-up table
Steps:
1: **for** i = 1: number of images
2: **for** $E_b/N_o = 0 : 0.5 : 3.5$
3: **for** CFs = 21:4:61
4: Calculate PSNR using Eq. (5)
Calculate SSIM using Eq. (6)
5: **end for**
6: Set CFs = 64
7: Calculate $PSNR_{max}$ and $SSIM_{max}$
8: Calculate Δ PSNR (i, E_b/N_o, CFs) = PSNR - $PSNR_{max}$
Δ SSIM (i, E_b/N_o, CFs) = SSIM- $SSIM_{max}$
9: **end for**
10: **end for**
11: Compute average Δ PSNR and average Δ SSIM for each E_b/N_o and CFs over all images
12: Select the best CFs at which Δ PSNR and Δ SSIM are maximized
13: Determine the transition value of E_b/N_o at which the best CFs changes
14: Construct look-up table between E_b/N_o and best CFs

The variation of Δ PSNR and Δ SSIM with E_b/N_o for the different number of CFs are shown in Fig.3. It is obvious that, for $E_b/N_o < 2\ dB$, superior number of CFs are 21 and for $E_b/N_o > 3\ dB$, Δ PSNR and Δ SSIM are negative values, hence the best number of CFs is 64. For $2\ dB \leq E_b/N_o \leq 3\ dB$, it is found that the best number of CFs is 33 coefficients. Concerning $E_b/N_o = 3$ dB, the Δ SSIM is approximately zero at number of CFs = 33 which means no gain is obtained in the SSIM value. However, the PSNR is improved by about 3dB. Therefore, the system suggests to utilize number of CFs=33 at $E_b/N_o = 3$ dB. Lastly, the proposed values of the best number of CFs for each E_b/N_o are presented in Table 2.

2) RICIAN AND RAYLEIGH FADING LOOK-UP TABLE

To construct look-up table for the fading channels, ***Algorithm1 is repeated except that*** E_b/N_o is varied from 0 to 28 dB. In addition, motivated by the results in the case of the AWGN channel, which show that no performance gain is achieved in the range of CFs from 33 to 61. Hence, we propose to vary the number of CFs from 21 to 33 in case of fading channels. Fig.4 shows the variation of Δ PSNR with E_b/N_o for the different values of CFs over the Rician channel with a fading factor (K= 4). It is obvious that 21 coefficients are superior for $0\ dB \leq E_b/N_o \leq 12\ dB$. For $12\ dB < E_b/N_o \leq 24\ dB$, 33 CFs are the best.

On the other hand, for $E_b/N_o > 24\ dB$, 64 coefficients are the best. However, Δ PSNR = 0.37 dB between 64 & 33 coefficients, this improvement is not strongly affecting the visual quality of the image. Moreover, $E_b/N_o = 26\ dB$ is not a practical value, hence we suggest using 33 CFs for $E_b/N_o > 24\ dB$. Therefore, in this scenario, the system uses only two chosen number of CFs as follows 21 coefficients is used for $0\ dB \leq E_b/N_o \leq 12\ dB$ and 33 coefficients is used for $E_b/N_o > 12\ dB$. Table 3 provides the best number of CFs for each E_b/N_o.

Algorithm 2 Rician Transition E_b/N_o Value Calculation

Inputs: Grey scale image dataset, Rician fading factors
Outputs: Transition value $(E_b/N_o)_{tr}$ at each fading factor
Steps:
1: **for** i = 1: number of images
2: **for** $K = 0 : 1 : 10$
3: **for** $E_b/N_o = 0 : 2 : 20$
4: Set CF = 21
5: Calculate PSNR using Eq. (5)
6: **end for**
7: Compute average PSNR over all images for each E_b/N_o
8: **end for**
9: **end for**
10: Repeat steps from 1 to 8 by setting CF=33
11: Find transition value of E_b/N_o at which average $PSNR_{33}$ - average $PSNR_{21} > 0$
12: Draw the transition value of E_b/N_o versus fading factors

To generalize the proposed look-up table for different fading factors, a relationship between the transition E_b/N_o value and Rician fading factor (K) must be determined. K varies from 0:10 [41], grey images are transmitted using 21 and 33 coefficients over the Rician channel with various fading factors.

The PSNR is computed for both cases, denoted by $PSNR_{21}$ and $PSNR_{33}$, respectively. The transition E_b/N_o is the value at which the system switches from transmitting 21 coefficients to 33 coefficients when the difference between average $PSNR_{33}$ and average $PSNR_{21}$ is positive. Steps of finding the transition E_b/N_o value $(E_b/N_o)_{tr}$ are summarized in Algorithm 2.

Fig.5 shows the plot of the transition E_b/N_o value resulted from the simulations. The relationship can be approximated by a linear model. It is obvious from Fig.5 that the transition value declines when K value increases. Since the fading factor K indicates the fading severity, if K=0 means Rayleigh fading (most severe fading), $K = \infty$ indicates no fading. Therefore, as the value of K increases, the quality of the channel improves. Consequently, the system can transmit an image with 33 coefficients at lower E_b/N_o value. The linear model depicted in Fig.5 can be approximated as follows:

$$(E_b/N_o)_{tr} = (E_b/N_o)_{tr}|_{K=0} - 2(K-1); \quad K \geq 1 \quad (7)$$

Therefore, the proposed system can easily calculate the transition E_b/N_o value for any fading factor using the above formula. It is to be mentioned that only look-up table in case of fading factor (K=0) is required to be able to use the above formula. The look-up table is constructed offline, once

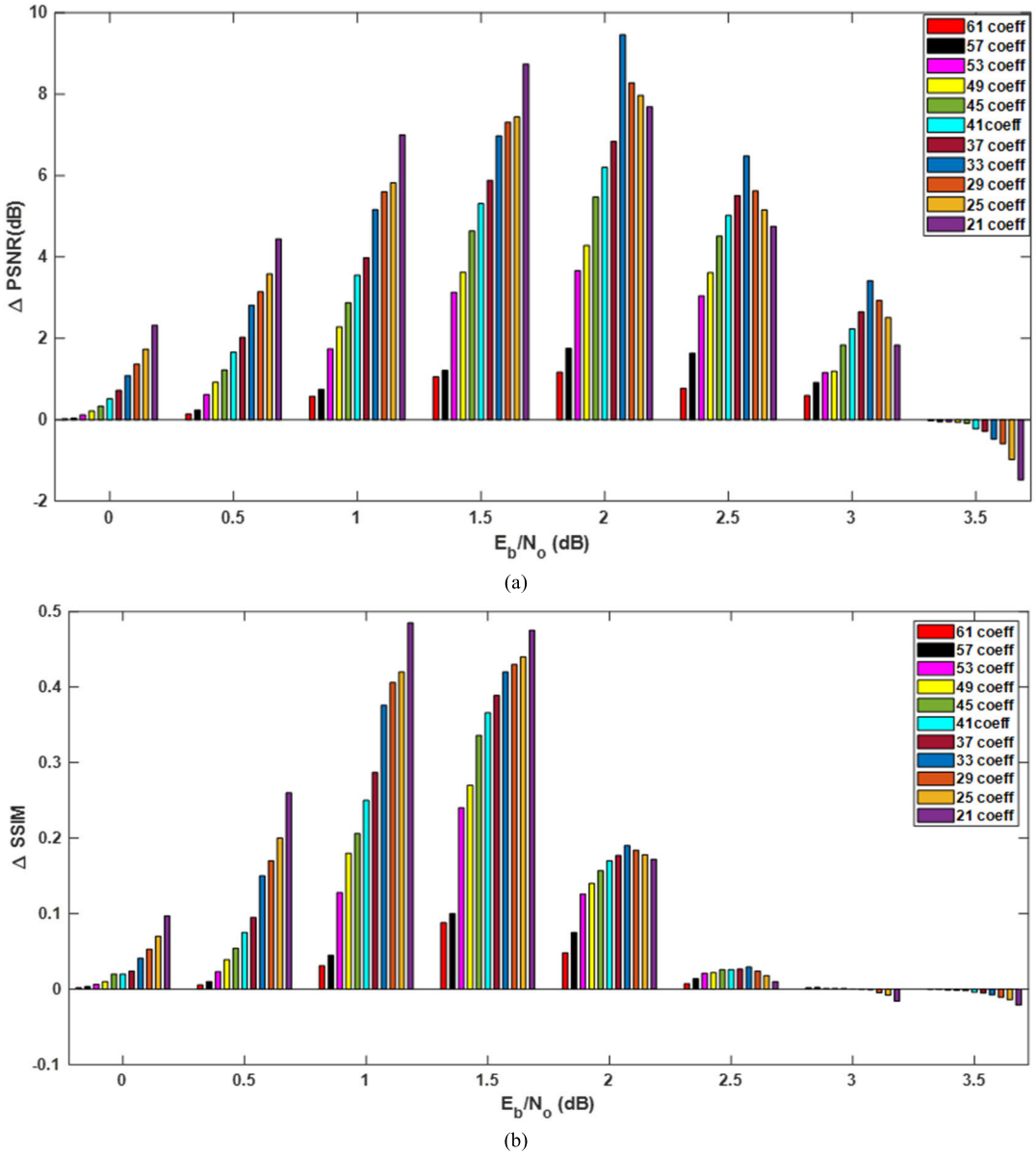

FIGURE 3. Performance evaluation versus E_b/N_o at different number of coefficients over AWGN channel: (a) Δ PSNR; (b) Δ SSIM.

TABLE 2. Proposed Look-up table for AWGN channel.

E_b/N_o (dB)	< 2	$2 \leq E_b/N_o \leq 3$	> 3
Number of coefficients	21	33	64

TABLE 3. Proposed Look-up table for RICIAN channel.

E_b/N_o (dB)	≤ 12	>12
Number of coefficients	21	33

finding the $(E_b/N_o)_{tr}$ value, the proposed system can adapt to any fading factor easily, which makes our proposed system fast and effective.

III. SIMULATION RESULTS

Extensive experiments are carried out in this section to validate the proposed system for image transmission over different communication channels. A comparison of the proposed system with a traditional digital-based communication system is also investigated. Moreover, the proposed system's performance is evaluated for images with different sizes.

A. SIMULATION SET-UP

Image dataset: The system is tested by using 20 greyscale images of size 256 × 256 pixels, available in [42] and [43].
Communication environment: The system is evaluated over AWGN and Rician channel with different fading factors and

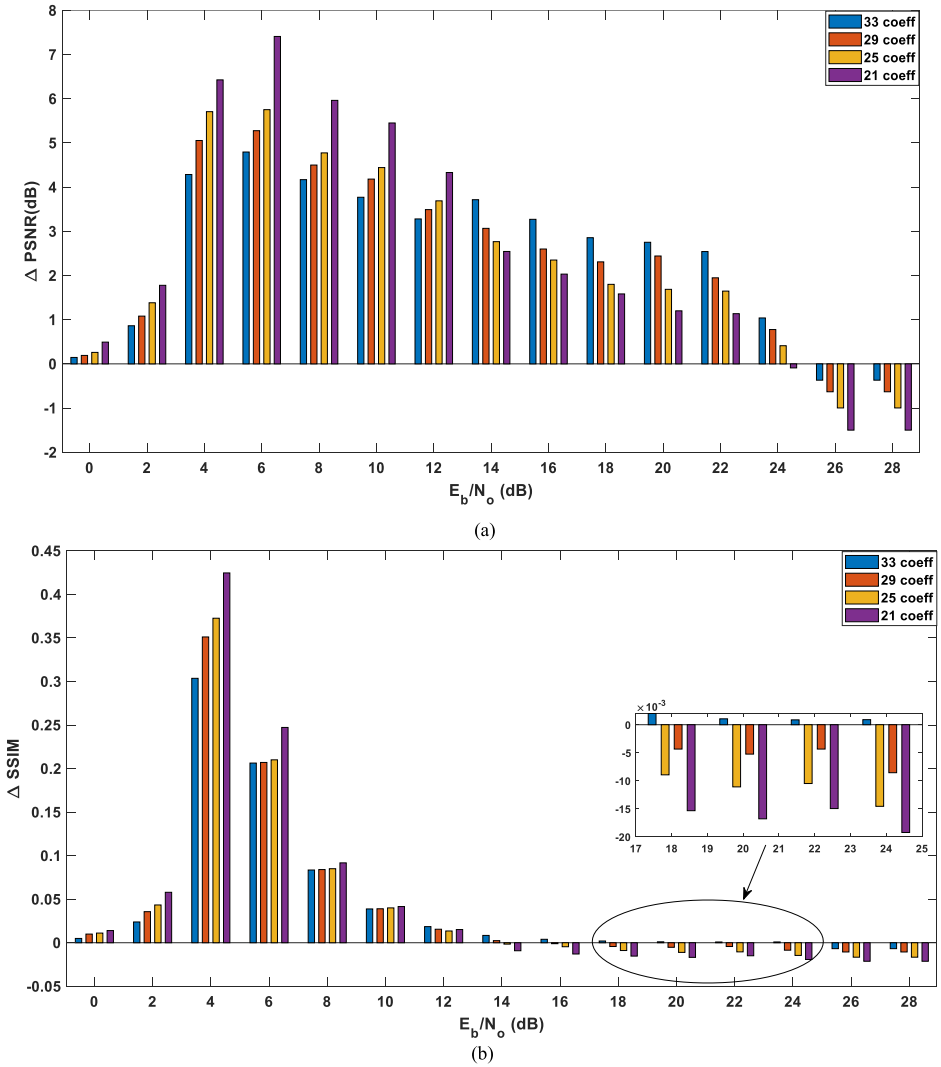

FIGURE 4. Performance evaluation versus E_b/N_o at different number of coefficients over Rician channel (K=4): (a) Δ PSNR; (b) Δ SSIM.

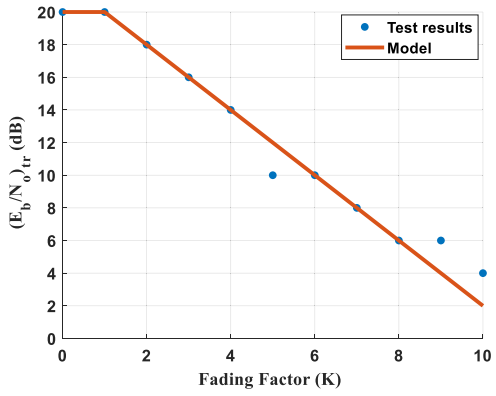

FIGURE 5. Relation between fading factors (K) and E_b/N_o.

Rayleigh channel, different E_b/N_o values are considered. BPSK modulation is adopted. In the proposed system, the codeword length of the used polar code is fixed and equals N=1024. Moreover, information bits M correspond to the binarized value of the selected CFs from look-up tables for a given E_b/N_o dB in case of AWGN. Accordingly, the obtained polar code rates are {168/1024, 264/1024, 512/1024}, that correspond to the transmitted number of CFs {21, 33, 64}, respectively. On the other hand, for transmission over Rician and Rayleigh channels, the system switches between two code rates {168/1024, 264/1024}, which correspond to the transmitted number of CFs {21, 33}, at transition E_b/N_o value that can be found from the proposed linear model for a given fading factor.

Metric: Every image from the dataset is transmitted many times to lessen the channel randomness effect. Performance is assessed in terms of PSNR and SSIM averaged over the images in the dataset. Moreover, the visual quality of the images is also presented.

Simulation settings are summarized in Table 4.

B. PERFORMANCE EVALUATION OVER AWGN CHANNEL

To study the robustness of the proposed system to the channel quality variations, Fig.6 provides the average PSNR and SSIM of the transmitted images versus the E_b/N_o for AWGN channel using the three mentioned code rates with the proposed adaptive rate polar code. Moreover, the proposed adap-

TABLE 4. Summary of the simulation settings.

Parameter	Value
Image size	256×256 pixels
Codeword length (N)	1024
Modulation type	BPSK
Channel model E_b/N_o (dB)	AWGN, Rician (K= 4,8), Rayleigh 0:0.5:4.5 (AWGN) 0:2:38 (Rician and Rayleigh)
Adaptive Polar code rate	{168/1024, 264/1024,512/1024} (AWGN) {168/1024, 264/1024} (Rician, Rayleigh)

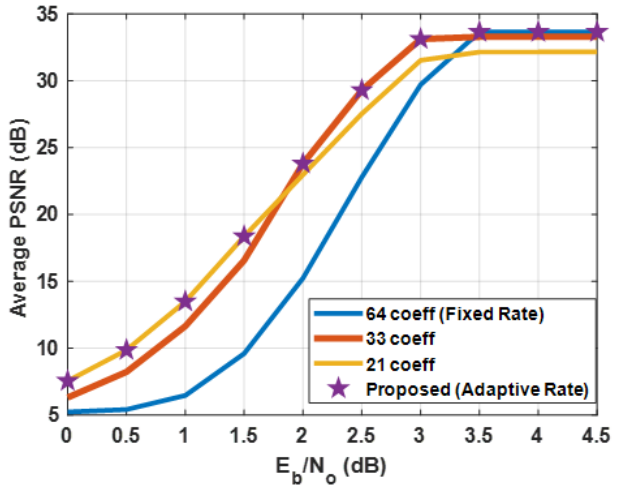

(a)

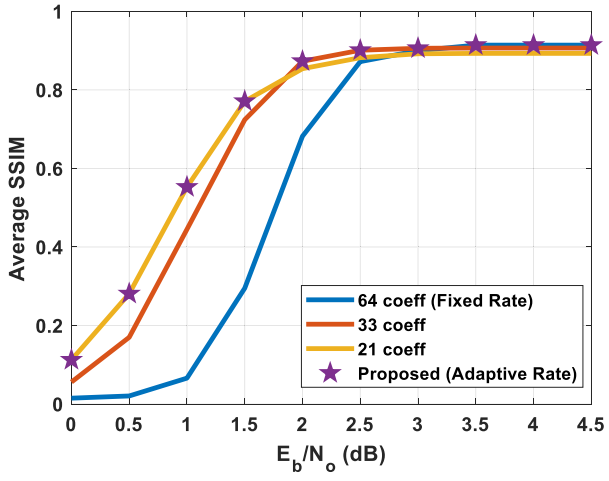

(b)

FIGURE 6. Objective performance evaluation of the proposed system over AWGN channel: (a) average PSNR versus E_b/N_o; (b) average SSIM versus E_b/N_o.

tive rate system is compared with the fixed code rate case, which corresponds to transmitting 64 coefficients.

It is shown that the proposed adaptive system can improve the quality of the reconstructed image under all channel conditions. Moreover, it can be observed that the adaptive rate system outperforms the fixed rate case by about 8 dB and 0.2 in PSNR and SSIM, respectively at $E_b/N_o = 2$dB.

Thereafter, the improvement gain gradually decreases, until the proposed system performance coincides with the fixed rate system at $E_b/N_o = 3.5$ dB. It can be further observed that, at $E_b/N_o = 3$ dB, the proposed system performance is approximately the same as the fixed rate system in terms of SSIM. However, the proposed adaptive system can improve the received image quality in terms of PSNR by approximately 3 dB.

Further, the subjective image quality of *Lena* image transmitted over AWGN using fixed rate polar code and the proposed adaptive rate system is shown in Fig.7. Right hand side presents the received images using the proposed system at $E_b/N_o = 1, 2$ and 3 dB. On the other hand, the received

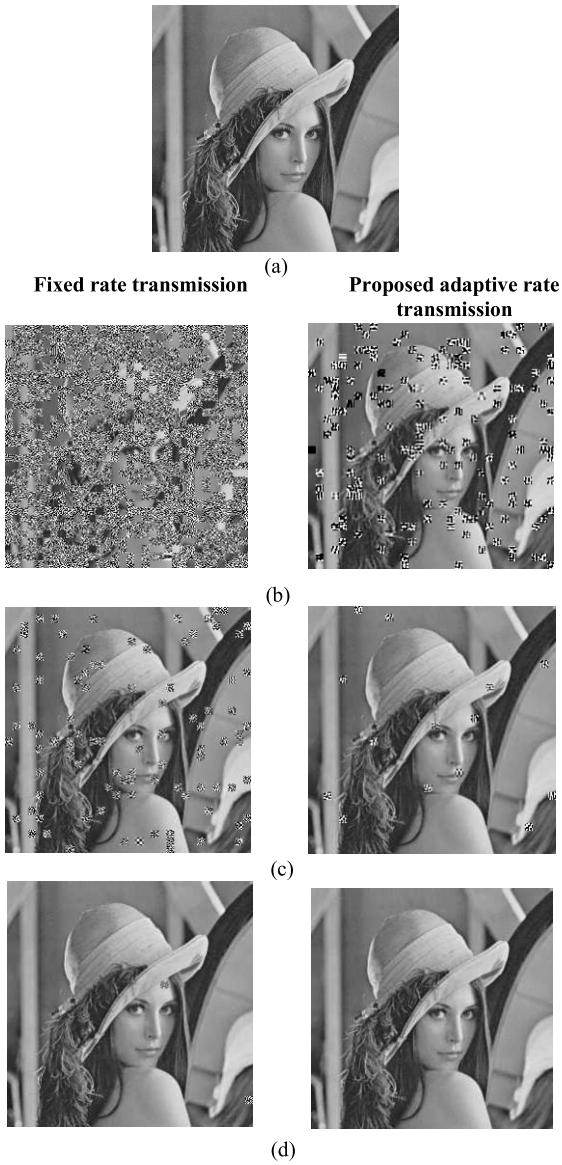

FIGURE 7. Subjective quality of reconstructed Lena image over AWGN; left hand side: fixed rate transmission. Right hand side: adaptive rate transmission: (a) Original image; (b) $E_b/N_o = 1dB$; (c) $E_b/N_o = 2dB$; (d) $E_b/N_o = 3dB$.

TABLE 5. Objective performance measures for example images over AWGN.

Image	E_b/N_o	Measures	Fixed rate polar code	Proposed adaptive rate polar code
Lena	1 dB	PSNR (dB)	6.88	**14.2**
		SSIM	0.079	**0.57**
	2 dB	PSNR (dB)	15.88	**23.77**
		SSIM	0.693	**0.867**
	3 dB	PSNR (dB)	29.23	**31.4**
		SSIM	0.896	**0.898**
Baboon	1 dB	PSNR (dB)	6.53	**13.39**
		SSIM	0.11	**0.49**
	2 dB	PSNR (dB)	15.41	**22.1**
		SSIM	0.68	**0.76**
	3 dB	PSNR (dB)	**25.16**	24.14
		SSIM	**0.83**	0.77
Bridge	1 dB	PSNR (dB)	6.66	**13.3**
		SSIM	0.10	**0.55**
	2 dB	PSNR (dB)	15.02	**22.68**
		SSIM	0.67	**0.82**
	3 dB	PSNR (dB)	27.02	**28.8**
		SSIM	0.879	**0.88**
Gold hill	1 dB	PSNR (dB)	6.7	**14.33**
		SSIM	0.077	**0.58**
	2 dB	PSNR (dB)	15.46	**23.87**
		SSIM	0.67	**0.842**
	3 dB	PSNR (dB)	29.59	**30.37**
		SSIM	0.87	0.87
Barbra	1 dB	PSNR (dB)	6.56	**13.67**
		SSIM	0.027	**0.54**
	2 dB	PSNR (dB)	14.9	**23.6**
		SSIM	0.69	**0.838**
	3 dB	PSNR (dB)	27.38	**28.03**
		SSIM	**0.914**	0.864

FIGURE 8. Comparison of visual quality for example images at E_b/N_o = 3 dB over AWGN channel: (a-d) fixed rate transmission; (e-h) proposed adaptive transmission.

images produced using a fixed rate are shown on the left-hand side. It is obvious that the visual image quality is significantly improved using the proposed adaptive rate polar code under all tested channel qualities.

Moreover, Table 5 compares the objective image quality in the two transmission scenarios by providing PSNR and SSIM values for *Lena, Baboon, Bridge, Goldhill* and *Barbra* images under different channel conditions. It can be concluded that the proposed system outperforms the fixed rate scenario under all tested channel qualities. However, at $E_b/N_o = 3$ dB, the proposed system PSNR is slightly higher than the fixed rate system, unlike the SSIM value, which is approximately the same for all example images except *Baboon and Barbra* images. The PSNR and SSIM values of *Baboon* image in the case of fixed rate transmission are higher than the proposed adaptive rate transmission by approximately 1 dB and 0.06, respectively.

On the other hand, the SSIM value of *Barbra* image in case of fixed rate transmission is higher than the proposed adaptive rate transmission by 0.05, but the proposed adaptive transmission is better in terms of PSNR.

Furthermore, to validate our pretension, Fig.8 compares the performance of the proposed system and the fixed rate system for *Baboon, Bridge, Gold hill*, and *Barbra* images at $E_b/N_o = 3$ dB. Fig.8(a-d) show the received images after being transmitted by the fixed rate polar code; on the other hand, Fig.8(e-h) present the proposed adaptive rate polar code results. Nevertheless, the visual quality of the *Baboon* image is better in the case of the proposed adaptive rate system, as shown in Fig.8e. Moreover, the reconstructed *Barbra* image has better visual quality in the case

of the proposed system as shown in Fig.8h. This analysis assures the robustness of the proposed adaptive rate transmission approach. Moreover, the visual quality of the received images using the proposed scheme is better than the fixed rate scheme for all the considered images. Finally, it can be noted that the proposed system attains acceptable visual quality under all channel qualities for different images.

C. PERFORMANCE EVALUATION OVER FADING CHANNELS

Further, we investigate the performance of the proposed system over Rician and Rayleigh fading channels with AWGN. Fig.9 illustrates the average PSNR and SSIM of the transmitted images versus the E_b/N_o of Rician channel with fading factors (K = 0,4,8) using the mentioned code rates. The proposed adaptive rate system achieves better performance than fixed rate code transmission. The performance of the proposed system gradually improves with respect to the channel quality. Moreover, it is obvious that the proposed system's performance improves as the value of the fading factor increases.

Furthermore, there is no noticeable difference between transmitting 64 CFS and 33 CFS when $E_b/N_o \geq 24$ dB shown for each fading factor. Hence, for simplicity, the proposed system adaptively switches between transmitting 21 CFs or 33 CFs according to the channel quality.

Fig.10 shows the visual quality of *lena* image transmitted over the Rician channel with a fading factor K = 4. Right-handed images present transmitted images with the proposed system, while transmitted images by fixed rate code system are on the left side. Clearly, the proposed system performance outperforms the fixed rate scheme at E_b/N_o = 4, 14 and 26 dB. Moreover, there is no difference between the received image using the proposed system and the fixed rate system at $E_b/N_o = 26\ dB$. This assures the robustness of the proposed system over diverse channel quality.

Furthermore, to subjectively evaluate the proposed system performance over various fading factors, Fig.11 demonstrates the visual quality of *peppers* image transmitted using the proposed system and fixed rate scheme over Rayleigh and Rician channels at E_b/N_o = 10 dB. The proposed system

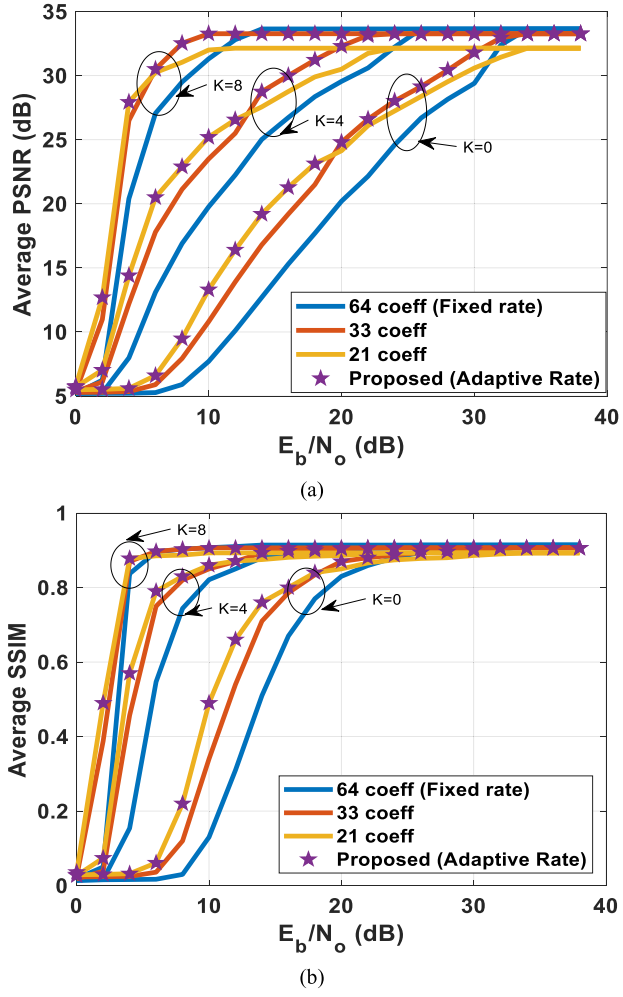

FIGURE 9. Objective performance evaluation of the proposed system over Rician fading channel (K=0,4,8): a) average PSNR versus E_b/N_o; b) average SSIM versus E_b/N_o.

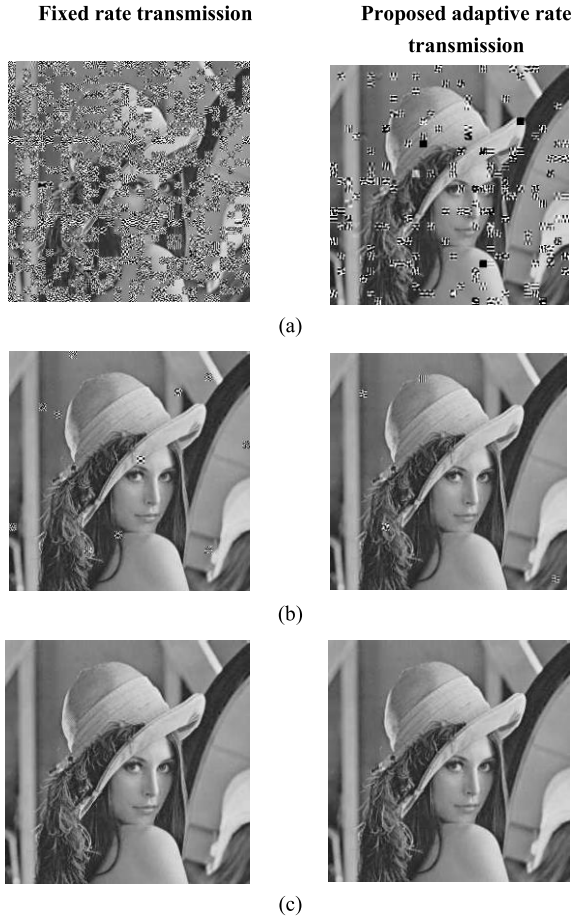

FIGURE 10. Subjective quality of Lena image over rician channel (K=4); left hand side: fixed rate transmission. Right hand side: adaptive rate transmission: (a) $E_b/N_o = 4dB$; (b) $E_b/N_o = 14dB$; (c) $E_b/N_o = 26dB$.

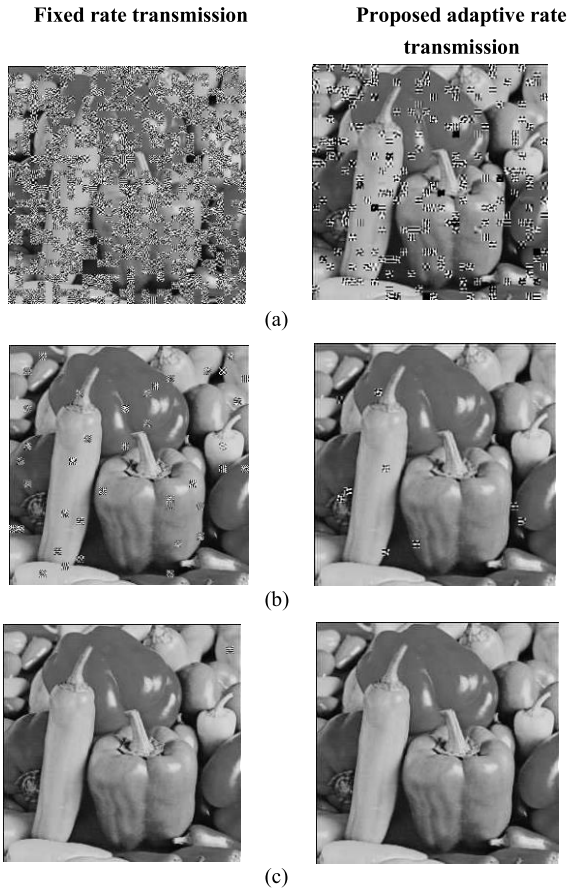

FIGURE 11. Subjective quality of peppers image over fading channel at $E_b/N_o = 10dB$; left hand side: fixed rate transmission. Right hand side: adaptive rate transmission; (a) K=0 (Rayleigh) (b) K=4 (c) K=8.

proves its robustness against various fading factors, as the visual quality of *peppers* image transmitted using the proposed system is better than those transmitted using a fixed rate code.

Moreover, to validate the performance of the proposed system over Rician fading channel (K=4), Table 6 presents PSNR and SSIM values of *Lena, Baboon, Bridge, Goldhill* and *Barbra* images at different channel quality. The proposed scheme outperforms the fixed rate scheme for all mentioned images at $E_b/N_o = 4, 14$ dB. However, at $E_b/N_o = 26$ dB, PSNR value of the images when transmitted by fixed rate code are higher than that transmitted by the proposed system. This is because the fixed rate utilizes all HF coefficients for the image reconstruction, and the proposed system uses only 12 HF coefficients in addition to LF coefficients. On the other hand, there is no big difference between the SSIM values of the two transmission schemes, this indicates no great visual quality variation between the two systems. Fig.12 demonstrates the visual quality of these images using both transmission schemes at $E_b/N_o = 26$ dB. No noticeable difference can be observed between right hand sided images (Proposed system) and left-hand sided images (fixed rate system), this confirms the suitability of the proposed system over Rician fading channel.

TABLE 6. Objective performance measures for example images over rician fading channel (k=4).

Image	E_b/N_o	Measures	Fixed rate polar code	Proposed adaptive rate polar code
Lena	4 dB	PSNR (dB)	8.17	**14.5**
		SSIM	0.15	**0.58**
	14 dB	PSNR (dB)	24.88	**28.17**
		SSIM	0.87	**0.88**
	26 dB	PSNR (dB)	**31.97**	31.4
		SSIM	**0.9**	0.898
Baboon	4dB	PSNR (dB)	8.16	**14.71**
		SSIM	0.21	**0.52**
	14dB	PSNR (dB)	22.1	**22.8**
		SSIM	0.68	**0.76**
	26 dB	PSNR (dB)	**25.98**	24.14
		SSIM	**0.835**	0.77
Bridge	4dB	PSNR (dB)	8.06	**14.67**
		SSIM	0.18	**0.61**
	14 dB	PSNR (dB)	22.78	**26.05**
		SSIM	0.84	**0.86**
	26dB	PSNR (dB)	**29.07**	28.8
		SSIM	0.88	0.88
Gold hill	4dB	PSNR (dB)	8.1	**14.5**
		SSIM	0.15	**0.57**
	14 dB	PSNR (dB)	23.9	**27.85**
		SSIM	0.845	**0.86**
	26 dB	PSNR (dB)	**30.63**	30.37
		SSIM	0.87	0.87
Barbra	4 dB	PSNR (dB)	8.03	**14.6**
		SSIM	0.17	**0.56**
	14 dB	PSNR (dB)	24.03	**26.66**
		SSIM	0.8	**0.85**
	26dB	PSNR (dB)	28.22	**28.87**
		SSIM	**0.91**	0.865

D. COMPARISON WITH TRADITIONAL DIGITAL-BASED SCHEME

In this section, the proposed system performance is compared with traditional digital-based scheme where the images are first compressed using the JPEG algorithm and then encoded by polar codes to reduce the channel distortion. For fair comparison, the JPEG compression factor is set to 50 such that the quantization matrix is similar to the one used in the proposed system, and Huffman codes are used in the entropy encoding stage. The compressed bit stream is then channel coded by polar codes with fixed code length of N=1024, However, we test with two different polar code rates, 0.5 and 0.75. We compare the average image quality expressed in terms of PSNR over the evaluation data set.

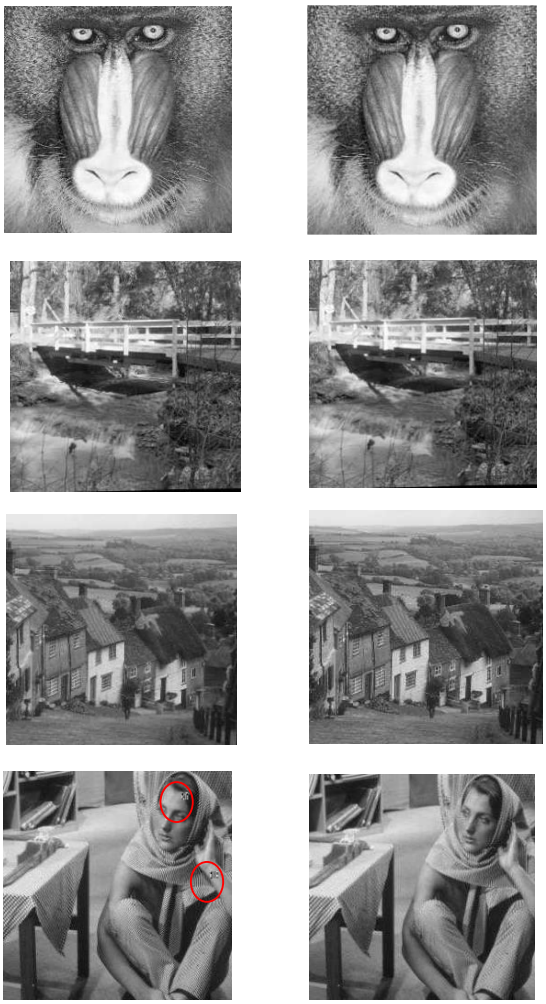

FIGURE 12. Comparison of visual quality for example images at E_b/N_o = 26 dB over rician fading channel (k=4) Left images: fixed rate transmission, right images: proposed system transmission.

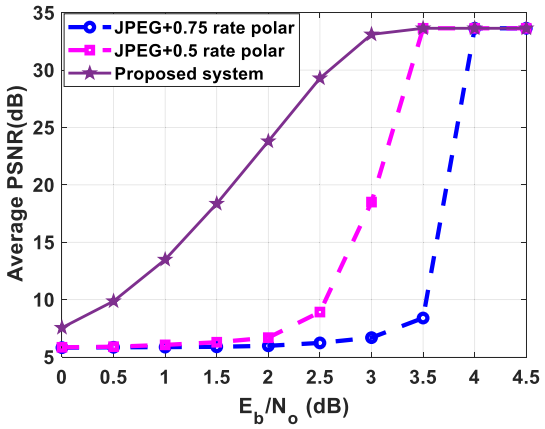

FIGURE 13. Comparison of adaptive rate proposed system with the traditional scheme using JPEG for source coding and polar codes for channel coding in AWGN channel.

The performance of the proposed system and the traditional transmission scheme in AWGN, Rician fading (K=4) and Rayleigh channels are shown in Fig 13-15, respectively. For the digital transmission scheme, a clear cliff effect exists

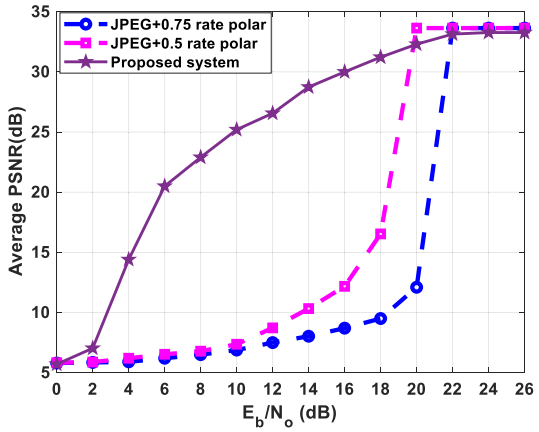

FIGURE 14. Comparison of adaptive rate proposed system with the traditional scheme using JPEG for source coding and polar codes for channel coding in fading channel (Rician fading factor=4).

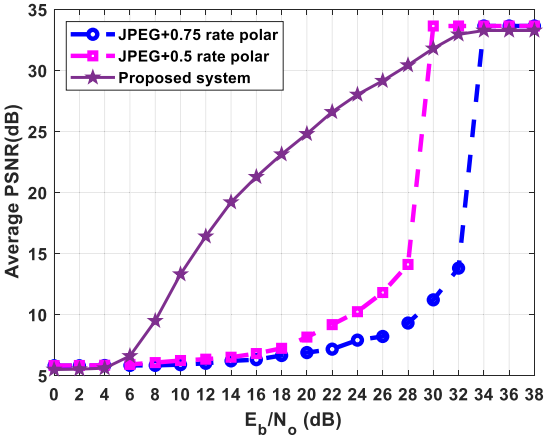

FIGURE 15. Comparison of adaptive rate proposed system with the traditional scheme using JPEG for source coding and polar codes for channel coding in Rayleigh channel.

for both channel code rates. For each polar code rate, there is a critical channel E_b/N_o value below which the image quality rapidly deteriorates and above which the reconstruction quality is fixed to the upper bound. This is determined by the comparison factor value in the JPEG codec. The results illustrate that the proposed system does not suffer from the cliff effect while exhibiting a graceful degradation in image quality when the channel quality decreases. Hence, the proposed algorithm is robust to channel quality fluctuations.

Moreover, the proposed system exhibits superior performance compared to digital-based transmission for the channel E_b/N_o value below the critical value at which the cliff effect occurs. The proposed system outperforms the digital-based transmission with polar code rates of 0.5 and 0.75 by 14, 25 dB at E_b/N_o = 3, 3.5 dB, respectively as shown in Fig13. This confirms that the proposed system does not suffer from a sudden decline in image quality. Furthermore, the proposed system outperforms the digital-based scheme at low E_b/N_o regions while performing similarly to the digital-based scheme at high E_b/N_o values over the AWGN channel scenario as shown in Fig.13.

Meanwhile, the proposed system has superior image quality compared to digital-based transmission scheme in low channel quality regions over Rician and Rayleigh channels. It is demonstrated from Fig.14 and Fig.15 that the proposed system performs better than traditional digital-based transmission scheme below the critical channel E_b/N_o value for both channel models. For Rician channel, the proposed system outperforms the digital-based transmission with polar code rate 0.5 by 14 dB at $E_b/N_o = 18$ dB and by 20 dB at $E_b/N_o = 20$ dB for rate 0.75. In addition, in Rayleigh channel, the proposed system outperforms by 15 dB at $E_b/N_o = 28$ dB for rate 0.5, and by 18 dB at $E_b/N_o = 32$ dB for rate 0.75.

Although it is obvious from Fig.14 and Fig.15 that the proposed system performance is inferior to the traditional digital-based transmission scheme at the critical E_b/N_o value, Fig.16 depicts that the proposed system achieves comparable SSIM values at the critical E_b/N_o value, indicating good perceived visual quality.

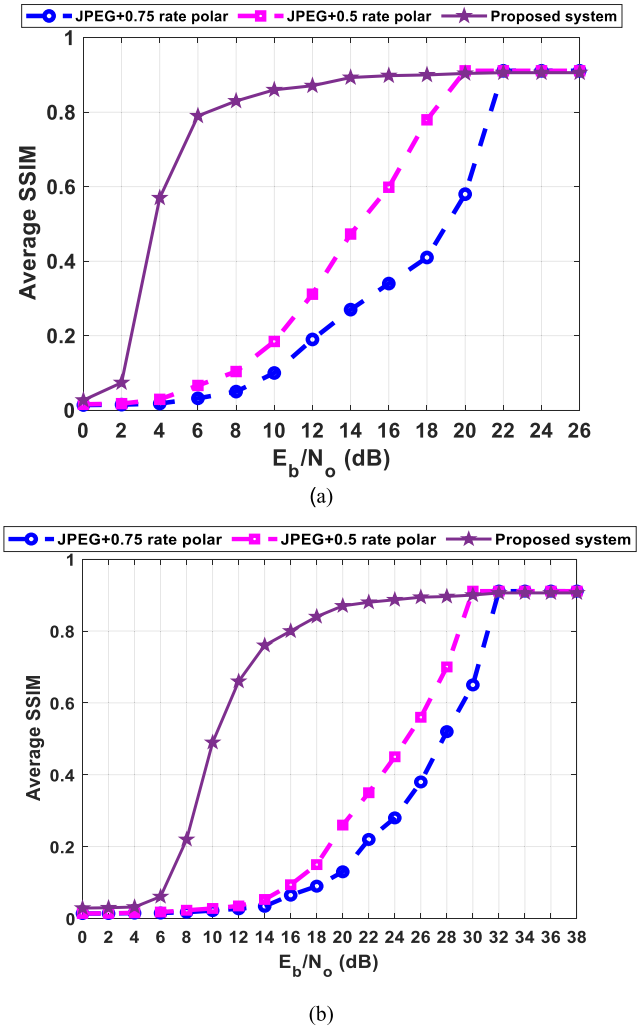

FIGURE 16. Comparison of adaptive rate proposed system with the traditional scheme using JPEG for source coding and polar codes for channel coding: (a) in Rician channel (Rician fading factor=4); (b) in Rayleigh channel.

Finally, visual comparison of the received cameraman image, as an example, using the proposed system and using traditional digital-based transmission with two code rates (0.5 and 0.75) is presented in Fig.17 for AWGN, Rician, and Rayleigh channels. For each received image, PSNR and

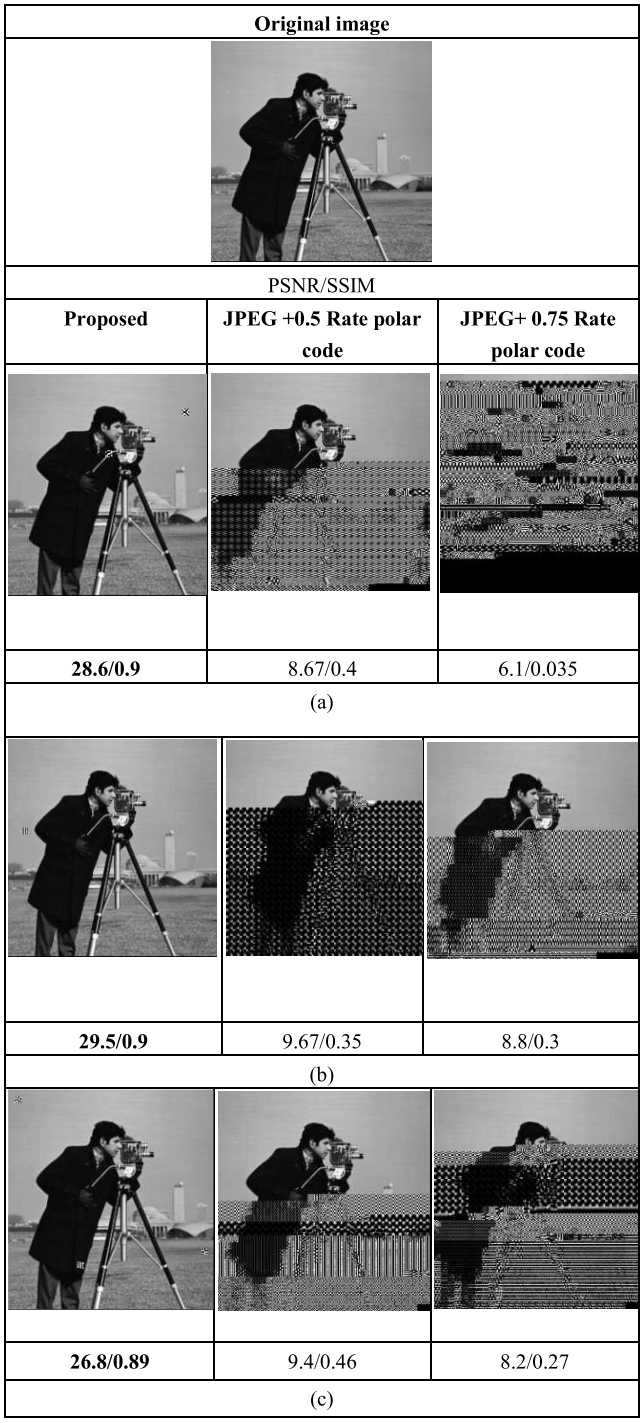

FIGURE 17. Visual comparison of adaptive rate proposed system with the traditional scheme using JPEG for source coding and polar codes for channel coding: (a) AWGN channel at $E_b/N_o = 2.5$dB; (b) Rician channel with fading factor= 4 at $E_b/N_o = 18$dB. (c) Rayleigh channel at $E_b/N_o = 22$dB.

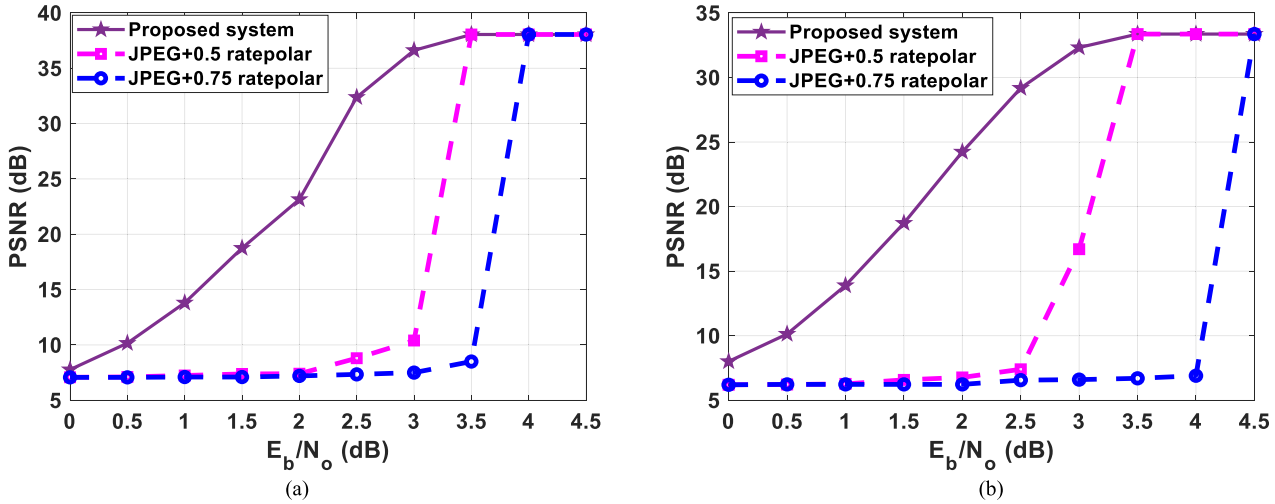

FIGURE 18. Performance of adaptive rate system for different sized images over AWGN channel: (a) Columbia image; (b) Man image.

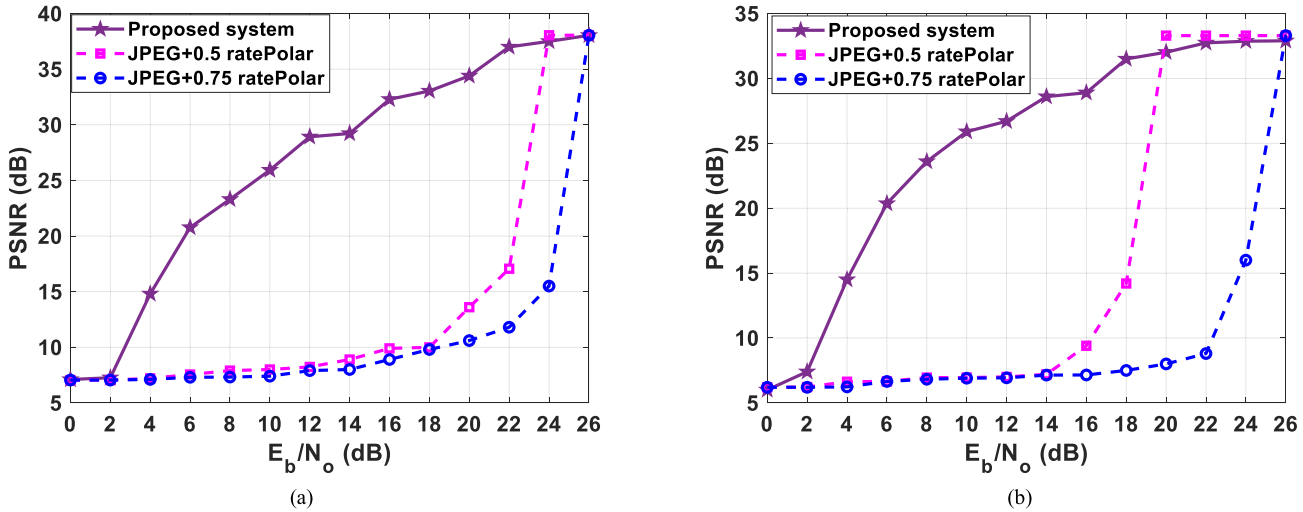

FIGURE 19. Performance of adaptive rate system for different sized images over Rician channel (K=4): (a) Columbia image; (b) Man image.

SSIM are reported. At the top of Fig.17, the original cameraman is presented. In the first row, the reconstructed images in AWGN channel at $E_b/N_o = 2.5$ dB are presented, the proposed system outperforms the traditional digital-based transmission with two different polar code rates; moreover, it is clear that the image is even unrecognizable in the case of using polar code rate 0.75. In the second and third rows, reconstructed images over Rician and Rayleigh channels are shown, respectively. Obviously, the proposed algorithm outperforms the traditional digital-based transmission scheme.

E. DIFFERENT SIZED IMAGES RESULTS

Without loss of generality, the proposed system is applied to different sized images. Two images were selected from [44], Columbia (480 × 480) and Man (512 × 512). Fig.18 compares the objective quality of two images when transmitted with the proposed adaptive system, and digital-based scheme over AWGN. The proposed system beats the digital-based transmission scheme at low channel quality, and the performance coincides with the traditional scheme at high channel quality. Similarly, Fig.19 illustrates the performance results in the case of Rician fading channel. This result validates the suitability of the proposed adaptive rate system for different sized images over various channel models.

IV. CONCLUSION

In this paper, an adaptive rate polar code has been proposed for image communication applications. The system utilizes the best number of DCT coefficients to be transmitted to achieve the best acceptable received image quality under all channel qualities. The results showed that the adaptive rate system has better performance than the fixed rate system. It was observed that the proposed system has outstanding performance compared with the traditional digital-based

scheme in different channel models. Simulation results reveal that under poor channel quality, better performance is more prominent for the proposed system. More significantly, the proposed system avoids the cliff effect that plagues traditional digital-based systems. Moreover, simulation results confirm the suitability of the proposed system for different sized images.

REFERENCES

[1] H. Qiu, G. Memmi, X. Chen, and J. Xiong, "DC coefficient recovery for JPEG images in ubiquitous communication systems," *Future Gener. Comput. Syst.*, vol. 96, pp. 23–31, Jul. 2019, doi: 10.1016/j.future.2019.01.037.

[2] S. Nandhini and K. Ashokkumar, "Machine learning technique for crop disease prediction through crop leaf image," *Appl. Math. Inf. Sci.*, vol. 16, no. 2, pp. 149–158, 2022, doi: 10.18576/amis/160202.

[3] A. S. Dar, S. Palanivel, M. K. Geetha, and M. Balasubramanian, "Mouth image based person authentication using DWLSTM and GRU," *Inf. Sci. Lett.*, vol. 11, no. 3, pp. 853–862, 2022, doi: 10.18576/isl/110317.

[4] S. Bakheet, M. Mofaddel, E. Soliman, and M. Heshmat, "Adaptive multimodal feature fusion for content-based image classification and retrieval," *Appl. Math. Inf. Sci.*, vol. 14, no. 4, pp. 699–708, 2020, doi: 10.18576/amis/140418.

[5] T.-Y. Tung, D. B. Kurka, M. Jankowski, and D. Gündüz, "Deep JSCC-Q: Constellation constrained deep joint source-channel coding," *IEEE J. Sel. Areas Inf. Theory*, early access, Dec. 23, 2022, doi: 10.1109/JSAIT.2022.3231042.

[6] S. Saravanan and M. Sivabalakrishnan, "Optimal image encryption in frequency domain using hybrid deer hunting with artificial bee colony with hybrid chaotic map," *Appl. Math. Inf. Sci.*, vol. 14, no. 6, pp. 1163–1174, 2020, doi: 10.18576/amis/140622.

[7] R. Sridevi and P. Philominathan, "Quantum colour image encryption algorithm based on DNA and unified logistic tent map," *Inf. Sci. Lett.*, vol. 9, no. 3, pp. 219–231, 2020, doi: 10.18576/isl/090309.

[8] G. K. Wallace, "The JPEG still picture compression standard," *IEEE Trans. Consum. Electron.*, vol. 38, no. 1, pp. 18–34, Feb. 1992, doi: 10.1109/30.125072.

[9] J. Balsa, T. Domínguez-Bolaño, Ó. Fresnedo, J. A. García-Naya, and L. Castedo, "Transmission of still images using low-complexity analog joint source-channel coding," *Sensors*, vol. 19, no. 13, p. 2932, Jul. 2019, doi: 10.3390/s19132932.

[10] M. Ding, J. Li, M. Ma, and X. Fan, "SNR-adaptive deep joint source-channel coding for wireless image transmission," in *Proc. IEEE Int. Conf. Acoust., Speech Signal Process. (ICASSP)*, Toronto, ON, Canada, Jun. 2021, pp. 1555–1559.

[11] T. Fujihashi, T. Koike-Akino, T. Watanabe, and P. V. Orlik, "Holo-Cast+: Hybrid digital-analog transmission for graceful point cloud delivery with graph Fourier transform," *IEEE Trans. Multimedia*, vol. 24, pp. 2179–2191, 2022, doi: 10.1109/TMM.2021.3077772.

[12] A. Li, T. Yang, W. Wu, and L. Luo, "Soft transmission of 3D video for low power and low complexity scenario," *Digit. Commun. Netw.*, May 2022, doi: 10.1016/j.dcan.2022.04.024.

[13] T. Fujihashi, T. Koike-Akino, and T. Watanabe, "Soft delivery: Survey on a new paradigm for wireless and mobile multimedia streaming," 2021, *arXiv:2111.08189*.

[14] Q. Chen, L. Wang, and S. Hong, "An image pre-processing approach for JSCC scheme based on double protograph LDPC codes," in *Proc. 16th Int. Symp. Commun. Inf. Technol. (ISCIT)*, Qingdao, China, Sep. 2016, pp. 109–112.

[15] L. Deng, Z. Shi, O. Li, and J. Ji, "Joint coding and adaptive image transmission scheme based on DP-LDPC codes for IoT scenarios," *IEEE Access*, vol. 7, pp. 18437–18449, 2019, doi: 10.1109/ACCESS.2019.2895368.

[16] Z. Xu, L. Wang, and S. Hong, "Joint early stopping criterions for protograph LDPC codes-based JSCC system in images transmission," *Entropy*, vol. 23, no. 11, p. 1392, Oct. 2021, doi: 10.3390/e23111392.

[17] Q. Mao, B. Xu, and Y. Qin, "A new scheme to improve the quality of compressed image transmission by turbo unequal error protection codes," in *Proc. 7th Int. Conf. Intell. Inf. Hiding Multimedia Signal Process.*, Dalian, China, Oct. 2011, pp. 226–229.

[18] L. Xu, L. Wang, S. Hong, and H. Wu, "New results on radiography image transmission with unequal error protection using protograph double LDPC codes," in *Proc. 8th Int. Symp. Med. Inf. Commun. Technol. (ISMICT)*, Apr. 2014, pp. 1–4.

[19] L. Chaari, M. Fourati, and L. Kamoun, "Image transmission quality analysis over adaptive Reed–Solomon coding," in *Proc. 15th IEEE Medit. Electrotechnical Conf. (Melecon)*, Valletta, Malta, Apr. 2010, pp. 409–414.

[20] M. S. Jassim and P. S. Boluk, "Reliable image transmission in wireless sensor networks for smart grid applications," in *Proc. 28th Signal Process. Commun. Appl. Conf. (SIU)*, Gaziantep, Turkey, Oct. 2020, pp. 1–4.

[21] H. Xu, K. Hua, and H. Wang, "Adaptive FEC coding and cooperative relayed wireless image transmission," *Digit. Commun. Netw.*, vol. 1, no. 3, pp. 213–221, Aug. 2015, doi: 10.1016/j.dcan.2015.05.002.

[22] M. Yigit, P. Sarisaray Boluk, and V. C. Gungor, "A new efficient error control algorithm for wireless sensor networks in smart grid," *Comput. Standards Interfaces*, vol. 63, pp. 27–42, Mar. 2019, doi: 10.1016/j.csi.2018.11.006.

[23] E. Arikan, "Channel polarization: A method for constructing capacity-achieving codes for symmetric binary-input memoryless channels," *IEEE Trans. Inf. Theory*, vol. 55, no. 7, pp. 3051–3073, Jul. 2009, doi: 10.1109/TIT.2009.2021379.

[24] A. Sharma and M. Salim, "Polar code appropriateness for ultra-reliable and low-latency use cases of 5G systems," *Int. J. Networked Distrib. Comput.*, vol. 7, no. 3, pp. 93–99, 2019, doi: 10.2991/ijndc.k.190702.005.

[25] V. Bioglio, C. Condo, and I. Land, "Design of polar codes in 5G new radio," *IEEE Commun. Surveys Tuts.*, vol. 23, no. 1, pp. 29–40, 1st Quart., 2021, doi: 10.1109/COMST.2020.2967127.

[26] O. Iscan, D. Lentner, and W. Xu, "A comparison of channel coding schemes for 5G short message transmission," in *Proc. IEEE Globecom Workshops (GC Wkshps)*, Washington, DC, USA, Dec. 2016, pp. 1–6.

[27] S. Belhadj and M. L. Abdelmounaim, "On error correction performance of LDPC and polar codes for the 5G machine type communications," in *Proc. IEEE Int. IoT, Electron. Mechatronics Conf. (IEMTRONICS)*, Toronto, ON, Canada, Apr. 2021, pp. 1–4.

[28] K. El-Abbasy, R. Taki Eldin, S. El Ramly, and B. Abdelhamid, "Optimized polar codes as forward error correction coding for digital video broadcasting systems," *Electronics*, vol. 10, no. 17, p. 2152, Sep. 2021, doi: 10.3390/electronics10172152.

[29] N. V. Krishna, P. P. Unnimaya, B. S. Anjana, V. B. Kumaravelu, and H. Jadhav, "Rate adaptive polar codes for 5G and beyond," in *Proc. Innov. Power Adv. Comput. Technol. (i-PACT)*, Kuala Lumpur, Malaysia, Nov. 2021, pp. 1–5.

[30] P. Shi, W. Tang, S. Zhao, and B. Wang, "Performance of polar codes on wireless communication channels," in *Proc. IEEE 14th Int. Conf. Commun. Technol.*, Chengdu, China, Nov. 2012, pp. 1134–1138.

[31] T. Payommai and K. Chamnongthai, "Performance of polar code for image transmission," in *Proc. Int. Symp. Intell. Signal Process. Commun. Syst.*, Naha, Japan, Nov. 2013, pp. 450–453.

[32] A. Mishra, K. Sharma, and A. De, "Quality image transmission through AWGN channel using polar codes," *Int. J. Computer Science and Telecommunications*, vol. 5, no. 1, pp. 8–16, 2014.

[33] A. Hadi, E. Alsusa, and A. Al-Dweik, "Information unequal error protection using polar codes," *IET Commun.*, vol. 12, no. 8, pp. 956–961, May 2018, doi: 10.1049/iet-com.2017.1195.

[34] K. Lay and H. Huang, "Digital image transmission with polar codes and median filtering," in *Proc. 4th Int. Conf. Intell. Green Building Smart Grid (IGBSG)*, Hubei, China, Sep. 2019, pp. 371–375.

[35] W. Du, S. Zhang, and F. Ding, "Exploiting the UEP property of polar codes to reduce image distortions induced by transmission errors," in *Proc. IEEE/CIC Int. Conf. Commun. China (ICCC)*, Shenzhen, China, Nov. 2015, pp. 1–5.

[36] Á. Garcia, M. D. L. M. G. Alcoforado, and F. Madeiro, "Improving image transmission by using polar codes and successive cancellation list decoding," *Ann. Disaster Risk Sci.*, vol. 3, no. 1, pp. 1–17, 2020, doi: 10.51381/adrs.v3i1.41.

[37] J. Hao, L. Liu, and W. Chen, "Performance of polar-coded 3D image transmission over fading channel," *Math. Problems Eng.*, vol. 2020, pp. 1–10, Jun. 2020, doi: 10.1155/2020/8403813.

[38] B. Furht, "Discrete Cosine Transform (DCT)," in *Encyclopedia of Multimedia*. Boston, MA, USA: Springer, 2006, pp. 203–205.

[39] *NR; Multiplexing and Channel Coding*, document TS 38.212, version 15.2.0, Release 15, 3GPP, 2018.
[40] Z. Wang, A. C. Bovik, H. R. Sheikh, and E. P. Simoncelli, "Image quality assessment: From error visibility to structural similarity," *IEEE Trans. Image Process.*, vol. 13, no. 4, pp. 600–612, Apr. 2004, doi: 10.1109/TIP.2003.819861.
[41] M. Alymani, M. H. Alhazmi, A. Almarhabi, H. Alhazmi, A. Samarkandi, and Y. Yao, "Rician K-factor estimation using deep learning," in *Proc. 29th Wireless Opt. Commun. Conf. (WOCC)*, Newark, NJ, USA, May 2020, pp. 1–4.
[42] R. C. Gonzalez, R. E. Woods, and S. L. Eddins. *Image Processing Place*. Accessed: Mar. 7, 2023. [Online]. Available: https://www.imageprocessingplace.com/root_files_V3/image_databases.htm
[43] University of Southern California, Signal and Image Processing Institute. (1977). *The USC-SIPI Image Database*. Accessed: Mar. 7, 2023. [Online]. Available: https://sipi.usc.edu/database/database.php?volume=sequences
[44] University of Cape Town. *Greyscale Standard Images*. Accessed: Mar. 7, 2023. [Online]. Available: https://www.dip.ee.uct.ac.za/imageproc/stdimages/greyscale/

MAI ADEL received the B.Sc. and M.Sc. degrees in electronics and communications engineering from the Faculty of Engineering, Ain Shams University, Cairo, Egypt, in 2012 and 2018, respectively, where she is currently pursuing the Ph.D. degree with the Faculty of Engineering. She is also a Mathematics Lecturer Assistant with German University in Cairo. Her research interests include image processing, communication systems, and coding.

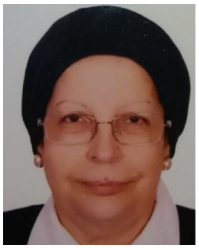

SALWA H. EL-RAMLY (Life Senior Member, IEEE) received the B.Sc. and M.Sc. degrees from the Faculty of Engineering, Ain Shams University, Egypt, in 1967 and 1972, respectively, and the Ph.D. degree from Nancy University, France, in 1976. She is currently an emeritus Professor with the Electronics and Communications Engineering Department, Faculty of Engineering, Ain Shams University, where she was the Head of the Department (2004–2006). She is also the President. She has published over 200 scientific papers and supervised more than 100 M.Sc. and Ph.D. theses. Her research interests include wireless communication systems and signal processing, language engineering, coding, encryption, and radars. She was awarded the Ain Shams Award of Appreciation in Engineering Sciences (2010), the Award of Excellence from the Society of Communications Engineers (2009), the Award of Excellence from the Egyptian Society of Language Engineering, and the Award of Appreciation from the National Radio Science Committee, Academy of Science Research and Technology, Cairo, Egypt, in 2018. She has been the IEEE Signal Processing Chapter Chair in Egypt, since 2003. She shared in the establishment of the Egyptian Society of Language Engineering, in 1996.

BASSANT ABDELHAMID (Senior Member, IEEE) received the B.Sc. and M.Sc. degrees in electronics and communications engineering from Ain Shams University, Egypt, in 2006 and 2010, respectively, and the Ph.D. degree in electronics and communications engineering from E-JUST University, in 2013. She has been an Associate Professor with the Faculty of Engineering, Ain Shams University, since May 2019. During the Ph.D. degree, she was a Special Research Student with Kyushu University, Japan. She was with Ain Shams University as an Assistant Professor, between 2013 and 2019. Her career history is about 15 years in total academic and research experiences in many universities which are Ain Shams University (ASU), Nile University (NU), British University in Egypt (BUE), and Université Française d'Égypte (UFE). She is supervising many master's and Ph.D. degree students. She is specialized in mobile and wireless communications engineering, digital signal processing, the Internet of Things (IoT), machine learning, and statistical signal processing. She has several international research publications, all in international journals with high impact factor and international conferences worldwide. She is also a reviewer in several high impact factor international journals and conferences. She is a Senior Member of the IEEE Communication Society and was the Chairperson of the IEEE Woman in Engineering (WIE) Egypt Section Affinity Group (2020–2022).